Fragmentation in Peripheral Heavy-Ion Collisions: from Neck Emission to Spectator Decays

J. Łukasik [a,j], G. Auger [b], M.L. Begemann-Blaich [a], N. Bellaize [d], R. Bittiger [a], F. Bocage [d], B. Borderie [c], R. Bougault [d], B. Bouriquet [b], J.L. Charvet [e], A. Chbihi [b], R. Dayras [e], D. Durand [d], J.D. Frankland [b], E. Galichet [c,k], D. Gourio [a], D. Guinet [f], S. Hudan [b], B. Hurst [d], P. Lautesse [f], F. Lavaud [c], A. Le Fèvre [a], R. Legrain [e,1], O. Lopez [d], U. Lynen [a], W.F.J. Müller [a], L. Nalpas [e], H. Orth [a], E. Plagnol [c], E. Rosato [g], A. Saija [h], C. Schwarz [a], C. Sfienti [a], J.C. Steckmeyer [d], B. Tamain [d], W. Trautmann [a], A. Trzciński [i], K. Turzó [a], E. Vient [d], M. Vigilante [g], C. Volant [e], B. Zwiegliński [i] and A.S. Botvina [a,l]

The INDRA and ALADIN Collaborations

[a] *Gesellschaft für Schwerionenforschung mbH, D-64291 Darmstadt, Germany*

[b] *GANIL, CEA et IN2P3-CNRS, F-14076 Caen, France*

[c] *Institut de Physique Nucléaire, IN2P3-CNRS et Université, F-91406 Orsay, France*

[d] *LPC, IN2P3-CNRS, ISMRA et Université, F-14050 Caen, France*

[e] *DAPNIA/SPhN, CEA/Saclay, F-91191 Gif sur Yvette, France*

[f] *Institut de Physique Nucléaire, IN2P3-CNRS et Université, F-69622 Villeurbanne, France*

[g] *Dipartimento di Scienze Fisiche e Sezione INFN, Univ. Federico II, I-80126 Napoli, Italy*

[h] *Dipartimento di Fisica dell' Università and INFN, I-95129 Catania, Italy*

[i] *A. Sołtan Institute for Nuclear Studies, Pl-00681 Warsaw, Poland*

[j] *H. Niewodniczański Institute of Nuclear Physics, Pl-31342 Kraków, Poland*

[k] *Conservatoire National des Arts et Métiers, F75141 Paris cedex 03, France*

[l] *Institute for Nuclear Research, 117312 Moscow, Russia*

Abstract

Invariant cross sections of intermediate mass fragments in peripheral collisions of ^{197}Au on ^{197}Au at incident energies between 40 and 150 MeV per nucleon have been measured with the 4π multi-detector INDRA. The maximum of the fragment production is located near mid-rapidity at the lower energies and moves gradually towards the projectile and target rapidities as the energy is increased. Schematic calculations within an extended Goldhaber model suggest that the observed cross-section distributions and their evolution with energy are predominantly the result of the clustering requirement for the emerging fragments and of their Coulomb repulsion from the projectile and target residues. The quantitative comparison with transverse energy spectra and fragment charge distributions emphasizes the role of hard scattered nucleons in the fragmentation process.

Key words: Symmetric heavy ion collision, Midrapidity emission, Goldhaber model, Coalescence, Hard scattering, Coulomb trajectory calculation
PACS: 25.70.Mn, 25.70.Pq, 25.40.Sc

The production of nuclear fragments is a decay mode that persists up to the highest bombarding energies in heavy-ion collisions. Its characteristics, however, are considerably different in the Fermi energy regime and in the relativistic regime. At bombarding energies near the Fermi energy, the fragment distributions are concentrated at mid-rapidity, neck breaking mechanisms have been suggested by various transport simulations, and strong Coulomb effects are generated by the presence of slowly moving heavy residues [1–14].

At relativistic energies, the fragment production in peripheral collisions is concentrated at projectile and target rapidities [15–17] with invariance properties that suggest a high degree of equilibration for the decaying spectator systems [18–20]. Because of their prevailing statistical character these fragmentations are often seen distinguished from the dynamical processes at intermediate energies.

The present study is directed to the transition region between these seemingly so different regimes with the aim to identify the basic ingredients that govern the evolution of the fragment production mechanisms. As the main result, we find that the same criteria are at work throughout the covered energy range and that, of these, the clustering (coalescence) criterion is essential for producing the observed features.

The experiments were performed at the GSI Darmstadt with beams of ^{197}Au, delivered by the heavy-ion synchrotron SIS and directed onto ^{197}Au targets

---

[1] deceased

of 2-mg/cm^2 areal thickness placed inside the INDRA multidetector [21]. The incident energies varied between 40 to 150 MeV per nucleon, a range of energies that corresponds to relative velocities between once and twice the Fermi value. Further details of the experimental and calibration procedures may be found in Refs. [22,23].

As described previously, the total transverse energy $E_\perp^{12}$ of light charged particles ($Z \leq 2$) has been used as an impact parameter selector [22]. The measured $E_\perp^{12}$ spectra scale linearly with the incident energy, and the scaled spectra coincide. The relation between $E_\perp^{12}$ and the reduced impact parameter $b/b_{\max}$ has been obtained by applying the geometrical prescription of Ref. [24]. It is linear in very good approximation, where $b/b_{\max}$ decreases with increasing $E_\perp^{12}$. Eight finite impact parameter bins were generated, with the most central bin 8 covering impact parameters up to 5% of $b_{\max}$. The remaining part of the $E_\perp^{12}$ spectrum has been divided into 7 bins of equal width, corresponding to 7 bins of approximately equal width in b, of which bin 1 contains the most peripheral events. An event was registered if at least three detectors had recorded a hit. The cross section covered with this trigger condition at, e.g., 40 MeV per nucleon amounted to 5.1 ± 0.8 b, as derived from the measured beam intensity, corresponding to $b_{\max} = 12.8 \pm 1.0$ fm in a sharp-cutoff approximation.

Invariant cross section distributions for lithium, carbon, and fluorine fragments emitted in peripheral ^{197}Au + ^{197}Au collisions are shown in Fig. 1. They illustrate the characteristic evolution of the emission pattern as the incident energy is raised from 40 up to 150 MeV per nucleon.

The Coulomb repulsion from the projectile and target residues that survive the collision at peripheral impact parameters is evident in all distributions. The distribution of intermediate-mass fragments, however, is not isotropic with respect to these residues. They are emitted with a preference toward mid-rapidity which produces a pronounced forward-backward asymmetry relative to the rapidities of the projectile and target residues. The resulting cross-section maximum at mid-rapidity at the lower energies gives way to a saddle-type structure at mid-rapidity at the higher energies. Here the fragment production is increasingly concentrated at the projectile and target rapidities, a trend that is more pronounced at even higher incident energies and generally characteristic for the relativistic regime [18]. At a given energy, the probability for forming fragments at mid-rapidity decreases rapidly with increasing Z.

The kinetic properties of the mid-rapidity fragments in peripheral collisions, in spite of this apparent evolution, have been found rather constant throughout the covered range of projectile energies [22]. The transverse velocities are invariant with respect to both, the incident energy and the fragment Z. This property and the large value $\langle E_t \rangle \approx 30$ MeV of the corresponding mean transverse energies were suggested to be the result of the combined action of the
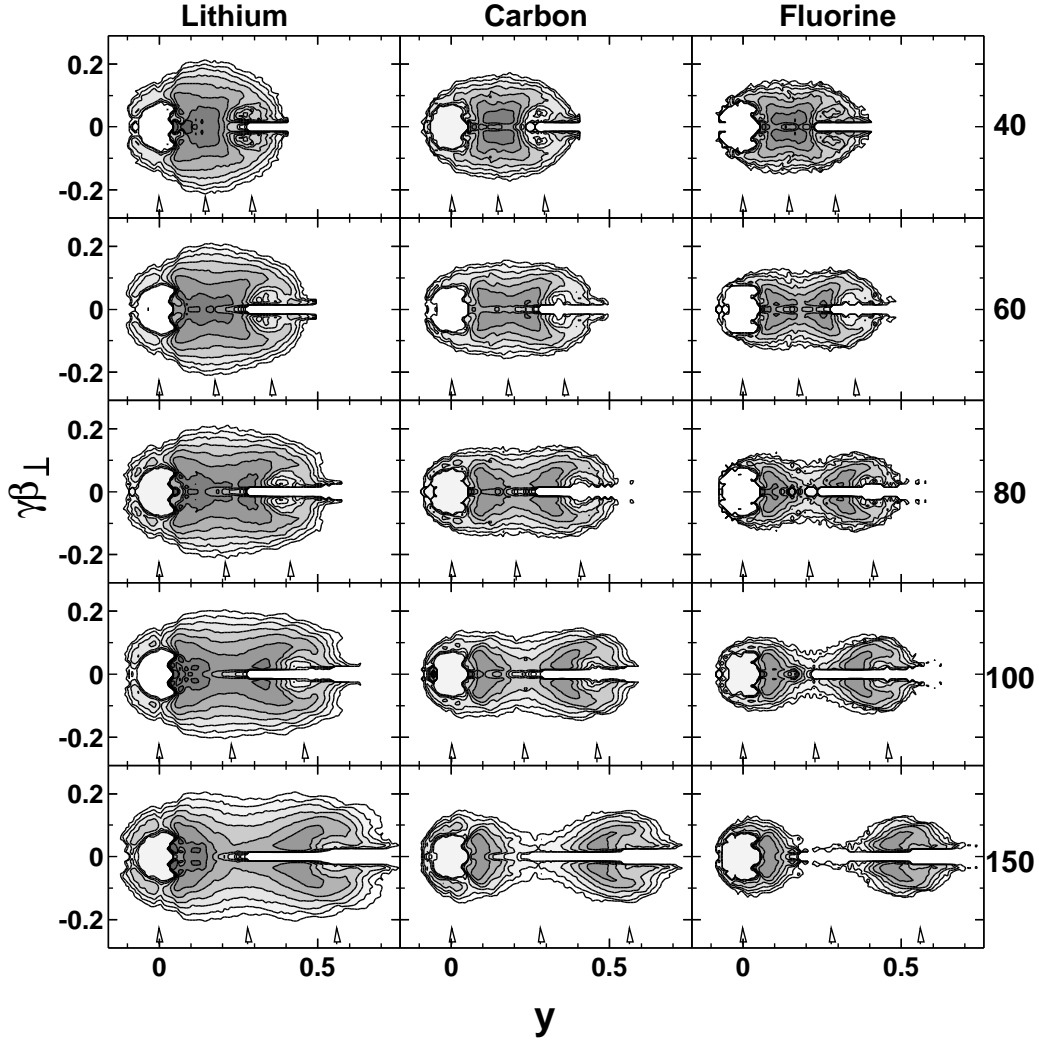
3

Fig. 1. Invariant cross section distributions as a function of transverse velocity $\gamma\beta_\perp$ and rapidity y for fragments with $Z = 3, 6, 9$ from the most peripheral collisions (bin 1) of $^{197}\text{Au} + ^{197}\text{Au}$ at $E/A = 40, 60, 80, 100$ and 150 MeV, as indicated. The cross sections are normalized relative to each other, separately for each fragment species. Near the target rapidity they are affected by the thresholds for fragment identification. The contour scale is logarithmic; the arrows indicate the target, center-of-mass and projectile rapidities (from left to right).

intrinsic Fermi motion, the acquired transverse energies of scattered nucleons and of the Coulomb repulsion from the heavy residues.

To obtain more quantitative predictions, a Monte-Carlo procedure based on these considerations has been developed. The original idea of Goldhaber [25] of taking the fragment momentum as the sum of the momenta of the constituent nucleons picked randomly from a single Fermi sphere has been extended by including also the Pauli-allowed distribution of hard scattered nucleons. The corresponding calculations proceed in three main steps:

4

(i) The momenta of the A nucleons of a fragment with mass number A are randomly picked from 2 Fermi spheres ($p_\mathrm{F} = 265$ MeV/c), separated by a relative momentum per nucleon calculated at the distance of closest approach of the two nuclei colliding at a given impact parameter, and also from the momentum distribution generated in hard two-body collisions of nucleons from the projectile and target. Isotropic scattering has been assumed for these collisions, and they were requested to obey the Pauli principle. The Pauli-allowed momentum space changes with increasing incident energy and widens both toward lower and higher transverse momenta. The number of hard scattered nucleons to be incorporated in a fragment was taken as a parameter. The results presented here were obtained assuming a binomial distribution of the number of hard scattered nucleons in a fragment with mean values that were found to be rather small (see below). For the entrance channel, two-body trajectory calculations with Coulomb and proximity forces [26] were performed. A fixed impact parameter of 10 fm was used; it corresponds approximately to the lower limit of bin 1, but its choice is not crucial.

(ii) A clustering criterion has been implemented by randomly accepting or rejecting the trial clusters according to the probability distribution of the mean squared relative momentum, $\sum_{i\neq j}(\vec{p}_i - \vec{p}_j)^2/(A(A-1))$, with that of A nucleons drawn randomly from a single Fermi sphere of the radius of $p_\mathrm{F} = 265$ MeV/c. Examples of these reference distributions are shown in the upper part of Fig. 2 for fragments containing 2, 7, 14, and 28 nucleons. They are characterized by a mean value $\langle p_\mathrm{rel}^2 \rangle$ and a variance $\sigma^2(p_\mathrm{rel}^2)$ given by:

$$\langle p_\mathrm{rel}^2 \rangle = \frac{6}{5}p_\mathrm{F}^2; \quad \sigma^2(p_\mathrm{rel}^2) = \frac{4}{25}p_\mathrm{F}^4 \frac{12A + 30}{7A(A-1)}.$$

The mean value of the distributions is constant while the variances decrease with increasing fragment mass A. The asymmetry apparent for lighter fragments disappears for heavier ones and, for $A \geq 7$, the distributions were approximated by Gaussians. The clustering criterion strongly suppresses the formation of fragments with large relative momenta of constituent nucleons.

The fragments selected by random picking of the momenta from a single Fermi sphere are not entirely cold (see e.g. [27]), and neither are the fragments defined with the above criterion. Temperatures deduced by fitting a Fermi distribution to the distribution of nucleon momenta in the center of mass of a fragment drops, approximately like $1/\sqrt{A}$, from about 5 MeV for $A = 10$ to near 0 for very large clusters. The sequential decay of excited clusters is expected to modify the fragment yields and kinetic energies, but not to an extent that would substantially modify the present conclusions.

The specific clustering criterion is adapted from the original Goldhaber formulation of the fragmentation problem by generalizing it from a single Fermi
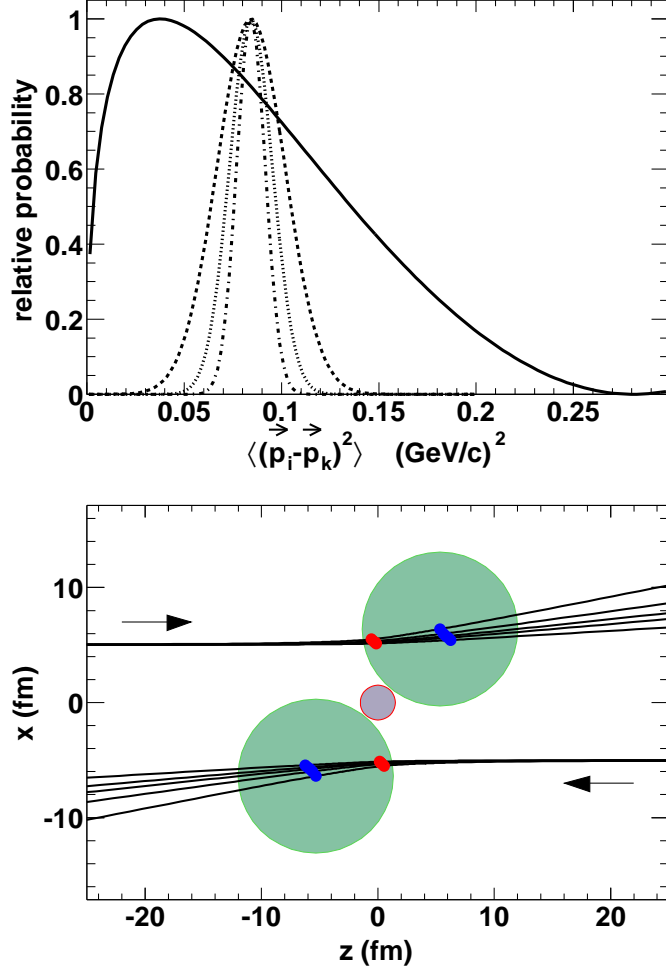
5

Fig. 2. Top panel: Distributions of relative probability of the mean squared relative momentum of nucleon pairs picked randomly from a single Fermi sphere for fragments with $A = 2$ (solid line) and Gaussian approximations of the distributions for $A = 7$, 14 and 28 (dashed, dotted and dash-dotted lines, respectively; all distributions are normalized to a maximum value of 1). Bottom panel: Initial spatial conditions for Coulomb trajectory calculations in the reaction plane, x vs z. The lines represent the trajectories of the projectile and the target at incident energies $E/A = 40$ to 150 MeV and for a fixed impact parameter of 10 fm. The dots placed on the trajectories mark the positions of the centers of the nuclei at the distance of closest approach (gray) and in the exit-channel sticking configuration (black). The arrows indicate the directions of the ion motion.

sphere to the three distributions considered here. It differs from standard coalescence criteria based on a fixed momentum radius and reduces the number of free parameters of the model as it depends only on p_F. Since neither the clustering in coordinate space nor the frequency of primary nucleon-nucleon scatterings are explicitly considered, only the effect on relative production probabilities can be studied.
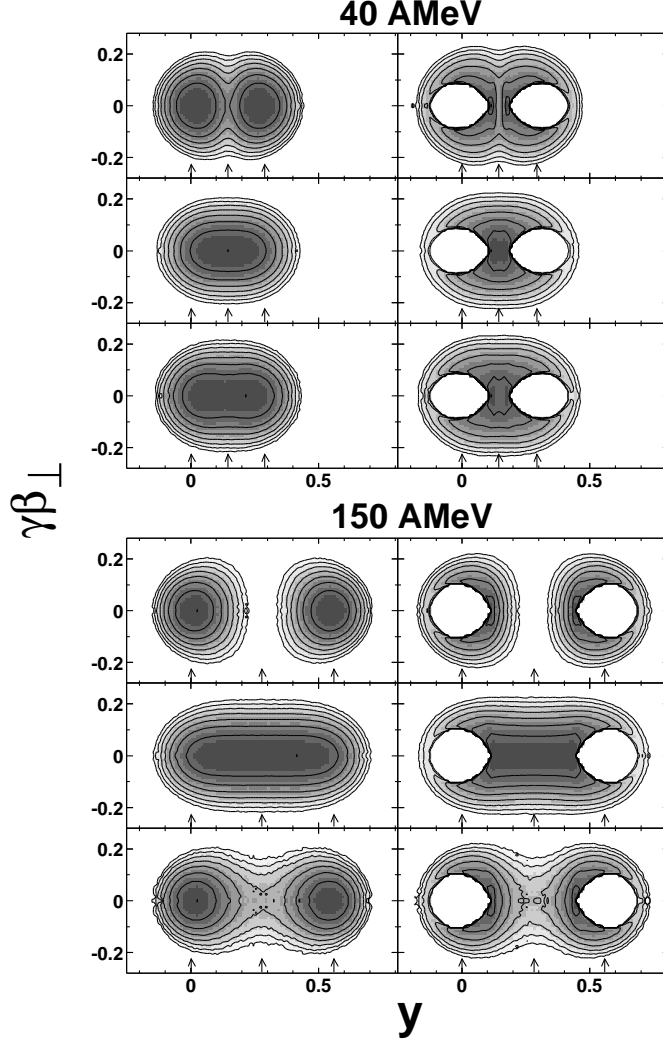
Fig. 3. Invariant cross sections of ^{7}Li fragments as a function of transverse velocity $\gamma\beta_\perp$ and rapidity y, as obtained from the model calculations for peripheral ^{197}Au + ^{197}Au collisions at $E/A = 40$ MeV (top part) and 150 MeV (bottom). The left and the right columns show the initial and asymptotic distributions, i.e. before and after the Coulomb trajectory calculations, respectively. The results without nucleon mixing, without the clustering criterion, and of the full calculation are shown in the top, middle, and bottom rows for both energies, respectively. The contour scale is logarithmic; the arrows have the same meaning as in Fig. 1.

(iii) Accepted fragments have been placed, in coordinate space, in between the two residues in an aligned sticking configuration which served as the starting point for 3-body Coulomb trajectory calculations (Fig. 2, bottom panel). The initial momentum of the produced fragment is determined by steps (i) and (ii), while the starting momenta of the two heavy fragments were taken from the trajectory calculations for the entrance channel. The residue trajectories remain virtually undisturbed in the exit channel. This simplified reaction picture assumes that the fragment is formed in the contact zone of the colliding

7

nuclei, where hard scattering takes place, and released as soon as the remaining residues separate by more than the diameter of the fragment which is assumed to be spherical. The effect of additional charged particles is ignored since their multiplicity in peripheral collisions is small.

The results obtained with this procedure for 40 and 150 MeV per nucleon, the lowest and highest bombarding energy included in this study, are shown in Fig. 3 for the case of fragments with mass number $A = 7$. Three different conditions were chosen for the calculations which all have the assumption in common that the number of hard scattered nucleons in a fragment is given by a binomial distribution with the mean value of 1. The resulting cross section distributions are rather similar at the lowest energy but become distinctively different as the energy is raised.
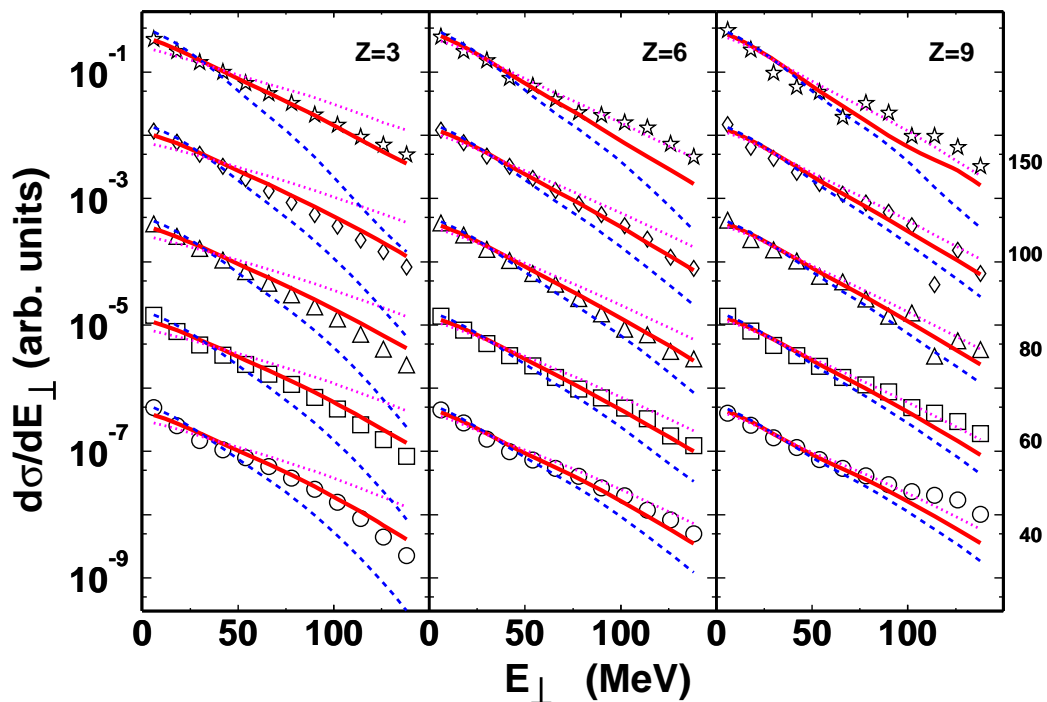

Fig. 4. Experimental (symbols) and calculated (lines) transverse-energy spectra of ^{7}Li (left panel), ^{13}C (middle), and ^{19}F fragments (right) emitted at mid-rapidity in peripheral ^{197}Au + ^{197}Au collisions at five incident energies, as indicated. Solid, dashed and dotted lines correspond to the calculations with on average one, zero or two scattered nucleons in a fragment, respectively. In each panel, the experimental spectra are displaced vertically by consecutive factors of 30, and the calculated spectra are individually normalized relative to the corresponding measurement.

If all the non-scattered nucleons forming a fragment are exclusively taken from only one of the collision partners, the mid-rapidity region cannot be populated at the higher bombarding energies (top row of Fig. 3 for 150 AMeV). At the lower energies (top row for 40 AMeV) these evaporation-like events are copiously found at mid-rapidity because the Coulomb maxima, forming

the characteristic rings in the two-dimensional representation, intersect. If the clustering criterion is dropped, (middle rows for both energies), the fragment distributions at high incident energies populate nearly homogeneously the full range from projectile to target rapidities, again in contrast to the observation (cf. Fig. 1). Both ingredients, the mixing of target and projectile nucleons (see also [6]) and the clustering criterion, are indispensable if more realistic distributions are to be generated that resemble those observed (bottom rows for both energies). The Coulomb field and its interplay with the initial momenta has a strong effect of rearranging and focusing the asymptotic fragments (cf. Ref. [11]). Their distribution extends to the projectile and target rapidities even though all fragments are initially placed in the aligned sticking configuration in between the two residues (see (iii) above). These specific initial conditions naturally produce the forward-backward asymmetry with respect to the heavy-residue rapidities.

For a more quantitative comparison, measured and calculated transverse-energy spectra for mid-rapidity fragments with $Z = 3, 6, 9$ are shown in Fig. 4. Bins centered at mid-rapidity with widths of 25% of the projectile rapidity y_p were chosen for the selection. The exponential spectra shapes correspond to normal statistical emissions. Only the high value of the mean transverse energy (≈ 30 MeV) has been found difficult to be explained within thermal models, as discussed in Ref. [22]. The shapes of these spectra, including their invariance with bombarding energy and Z, are rather well reproduced if on average one scattered nucleon from the Pauli-allowed distribution of hard scattered nucleons is included in the fragment (solid lines). If scattered nucleons are excluded (dashed lines) or if their mean number is increased to 2 (dotted lines), the resulting spectra deviate significantly from the experiment, in particular for the lighter fragments.

The small number of scattered nucleons in a fragment is consistent with the relatively small number of primary nucleon-nucleon collisions expected for the very peripheral collisions selected with bin 1 but also reflects a small probability for a hard-scattered nucleon to become part of a fragment. The total multiplicity of intermediate-mass fragments in bin 1 at, e.g., 40 MeV per nucleon is 0.5, while the average geometrical fireball [28] in this bin contains about 20 participant nucleons. The increasingly harder transverse-energy spectra in more central collisions [22] require more scattered nucleons to be included, in particular at the higher incident energies. For 100 and 150 MeV per nucleon, the lithium spectra of bins 2 and 3, e.g., are well described if their mean number in a fragment is increased to 1.5 and 2, respectively.

The general trends of the experimental cross section distributions as a function of the fragment Z are also rather well reproduced. This is demonstrated in Fig. 5 for the range of mid-rapidity fragments with 3≤Z≤10. The Z distributions are approximately exponential functions with slopes that increase

9

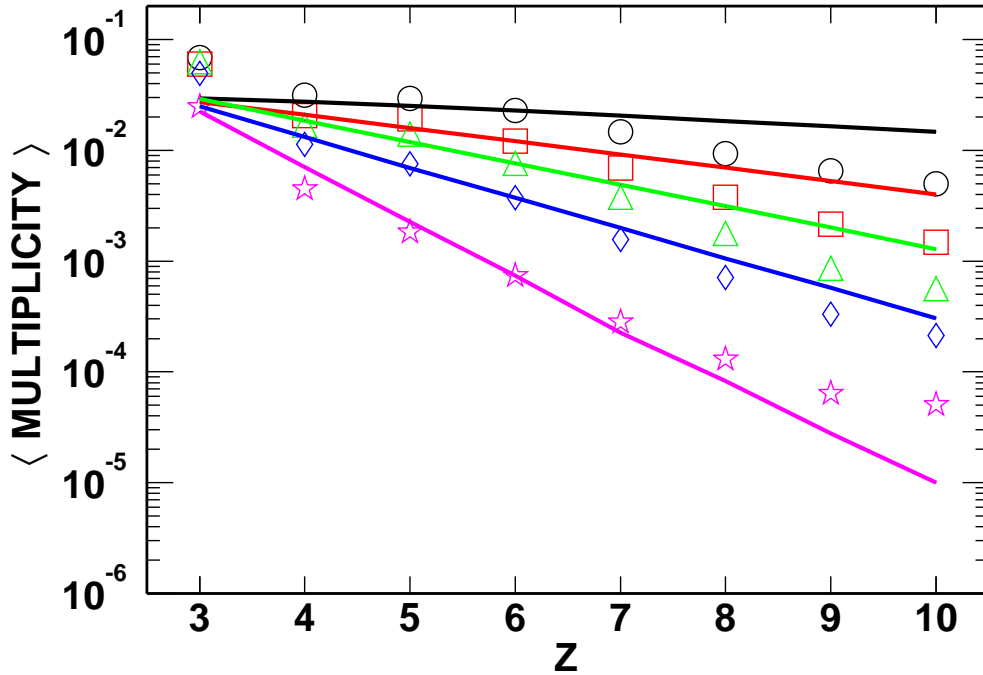Fig. 5. Experimental (symbols) and calculated (lines) mean multiplicity of mid-rapidity fragments in peripheral ^{197}Au + ^{197}Au collisions (bin 1) as a function of Z. The calculated spectra are normalized at $Z = 6$, separately for each of the five bombarding energies $E/A = 40, 60, 80, 100, 150$ MeV (from top to bottom).

monotonically with the incident energy. The calculations have been performed for masses $A = 2Z+1$ and for, on average, one scattered nucleon in a fragment. The Z dependence of the differential multiplicities is nearly perfectly reproduced for 100 MeV per nucleon but the variation of the slopes with incident energy is slightly overpredicted. With the chosen normalization at $Z = 6$, this has the effect that the yields of the heavier fragments are underestimated at the highest and overestimated at the lower bombarding energies. The yields of lithium fragments are also too low by about a factor of two at all energies except 150 MeV per nucleon, where the measured yields are lower. Overall, however, the agreement is very satisfactory.

From the good qualitative (Figs. 1 and 3) and quantitative agreement (Figs. 4 and 5) we may thus conclude that the presented extended Goldhaber scenario contains the essential ingredients of the fragmentation mechanism in peripheral collisions. Of these, the clustering criterion is responsible for the evolution of the cross section distributions from mid-rapidity to the spectator rapidities with increasing projectile energy. It is furthermore important to permit the mixing of projectile and target nucleons and to include hard-scattered nucleons from Pauli-allowed collisions into the produced fragments. This latter observation even suggests the hypothesis that the hard-scattered nucleons may be required for initiating the fragment production at mid-rapidity in

peripheral collisions. The correct prediction of the role of scattered nucleons may therefore be considered as an important test for any dynamical model to describe the mid-rapidity emission. It is, finally, remarkable how far the fragment distributions extend into the projectile and target rapidity regions, as a consequence of the combined action of the initial momenta and of the Coulomb forces giving rise to the characteristic ring structures. Apparently, fragments observed there do not necessarily have to be considered as emitted from the excited residues but may to a large part originate from the contact zone, or neck region, formed during the reaction.

References

[1] C.P. Montoya *et al.*, Phys. Rev. Lett. **73** (1994) 3070.

[2] J. Tõke *et al.*, Phys. Rev. Lett. **75** (1995) 2920.

[3] M. Colonna *et al.*, Nucl. Phys. **A589** (1995) 160.

[4] J.F. Dempsey *et al.*, Phys. Rev. C **54** (1996) 1710.

[5] J. Łukasik *et al.*, Phys. Rev. C **55** (1997) 1906.

[6] R. Nebauer and J. Aichelin, Nucl. Phys. **A650** (1999) 65.

[7] E. Plagnol *et al.*, Phys. Rev. C **61** (2000) 014606.

[8] D. Doré *et al.*, Phys. Rev. C **63** (2001) 034612.

[9] G. Poggi, Nucl. Phys. **A685** (2001) 296c.

[10] A.S. Botvina and I.N. Mishustin, Phys. Rev. C **63** (2001) 061601(R).

[11] S. Piantelli *et al.*, Phys. Rev. Lett. **88** (2002) 052701.

[12] P. M. Milazzo *et al.*, Nucl. Phys. **A703** (2002) 466.

[13] V. Baran *et al.*, Nucl. Phys. **A703** (2002) 603.

[14] B. Davin *et al.*, Phys. Rev. C **65** (2002) 064614.

[15] J. Hubele *et al.*, Phys. Rev. C **46** (1992) R1577.

[16] J.A. Hauger *et al.*, Phys. Rev. Lett. **77** (1996) 235.

[17] Hongfei Xi *et al.*, Z. Phys. A **359** (1997) 397; Eur. Phys. J. A **1** (1998) 235

[18] A. Schüttauf *et al.*, Nucl. Phys. **A607** (1996) 457.

[19] T. Gaitanos *et al.*, Phys. Lett. B **478** (2000) 79.

[20] A. Insolia *et al.*, Phys. Rev. C **61** (2000) 044902.

[21] J. Pouthas *et al.*, Nucl. Instr. Meth. in Phys. Res. **A357** (1995) 418.

[22] J. Łukasik *et al.*, Phys. Rev. C **66** (2002) 064606.

[23] A. Trzciński *et al.*, Nucl. Instr. Meth. in Phys. Res. **A501** (2003) 361.

[24] C. Cavata *et al.*, Phys. Rev. C **42** (1990) 1760.

[25] A.S. Goldhaber, Phys. Lett. **53B** (1974) 306.

[26] C. Ngô *et al.*, Nucl. Phys. **A252** (1975) 237.

[27] M.J. Murphy, Phys. Lett. **135B** (1984) 25.

[28] J. Gosset *et al.*, Phys. Rev. C **16** (1977) 629.